WILEY-VCH

DOI: 10.1002/ ((please add manuscript number))
Article type: Communication

Hollow TiO_2@Co_9S_8 Core-Branch Arrays as Bifunctional Electrocatalysts for Efficient Oxygen/Hydrogen Production

以空心 TiO2_Co9S8 点线阵列作为双功能电催化剂,用于高效氧气/氢气生产

Shengjue Deng, Yu Zhong, Yinxiang Zeng, Yadong Wang, Xiuli Wang, Xihong Lu, Xinhui Xia*, and Jiangping Tu*

S. J. Deng, Y. Zhong, Prof. X. L. Wang, Prof. X. H. Xia, Prof. J. P. Tu,
State Key Laboratory of Silicon Materials,
Key Laboratory of Advanced Materials and Applications for Batteries of Zhejiang Province,
and Department of Materials Science and Engineering,
Zhejiang University,
Hangzhou 310027, P. R. China.
E-mail: helloxxh@zju.edu.cn

Y. X. Zeng, Prof. X. H. Lu,
MOE of the Key Laboratory of Bioinorganic and Synthetic Chemistry, KLGHEI of Environment and Energy Chemistry, School of Chemistry,
Sun Yat-Sen University,
Guangzhou 510275, China.
E-mail: luxh6@mail.sysu.edu.cn

Dr. Yadong Wang
School of Engineering, Nanyang Polytechnic,
569830, Singapore

Keywords: cobalt sulfide; arrays; electrochemical water splitting; hydrogen evolution reaction; oxygen evolution reaction

Abstract: Designing ever more efficient and cost-effective bifunctional electrocatalysts for oxygen/hydrogen evolution reactions (OER/HER) is greatly vital and challenging. In this work, we develop a new kind of binder-free hollow TiO_2@Co_9S_8 core-branch arrays as highly active OER and HER electrocatalysts for stable overall water splitting. Hollow core-branch arrays of TiO_2@Co_9S_8 are readily realized by the rational combination of cross-linked Co_9S_8 nanoflakes on TiO_2 core via a facile and powerful sulfurization strategy. Arising from larger active surface area, richer/shorter transfer channels for ions/electrons and reinforced structural stability, the as-obtained TiO_2@Co_9S_8 core-branch arrays show noticeable exceptional electrocatalytic performance, with low overpotentials of 240 and 139 mV at 10 mA cm^{-2} as well as low Tafel slopes of 55 and 65 mV Dec^{-1} for OER and HER in alkaline medium, respectively. Impressively, the electrolysis cell based on the TiO_2@Co_9S_8 arrays as both cathode and anode exhibits a remarkably low water splitting voltage of 1.56 V at 10 mA cm^{-2} and long-term durability with no decay after 10 days. Our versatile fabrication protocol and smart branch-core design provide a new way to construct other advanced metal sulfides for energy conversion and storage.

1. Introduction

Developing green fuel technology is critical for energy security and sustainable development of social economy. Electrochemical water splitting is recognized as a highly potential technology to convert electricity into environment-friendly and renewable chemical fuels (hydrogen and oxygen).[1-3] The cathodic hydrogen evolution reaction (HER) and anodic oxygen evolution reaction (OER) depend heavily on the development of cost-effective high-performance electrocatalysts.[4, 5] Currently, platinum (Pt)/Pt-based alloy and iridium/ruthenium oxides (IrO_2/RuO_2) are considered as the most promising electrocatalysts for HER and OER, respectively, but their scarcity, high cost and compromised stability hinder their widespread applications.[6, 7] Additionally, the best working situation for those OER and HER catalysts is often mismatchable since OER preferably takes place in alkaline or neutral solution while HER in acidic medium.[8, 9] This would cause compromised performance for overall water splitting. For instance, the commercial alkaline electrolyzers require high cell voltages (1.8-2.0 V) to drive water splitting,[10] far ahead of the theoretical value of ~1.23 V owing to high overpotentials on the sluggish of OER and HER. Therefore, it is highly desirable to explore alternative high-performance and low-cost bifunctional OER/HER electrocatalysts for overall water splitting.[11-15]

Over the past decades, great progress has been achieved on the development of non-noble metal-based electrocatalysts for both OER and HER. Various nonprecious metal oxides,[9] sulfides,[16] selenides,[17] phosphides and nitrides,[18, 19] have been exploited. Among these electrocatalysts, cobalt sulfide (Co_9S_8) is regarded as an attractive electrocatalyst for water splitting due to its high catalytic activity for HER and OER simultaneously, and excellent electrochemical stability. In comparison to bulk Co_9S_8, nanostructured Co_9S_8 and its composites could afford more active sites and faster transfer rate of ions/electrons during the electrocatalytic reaction, and thus usually exhibiting enhanced HER and OER activities.[20-24] Currently, several Co_9S_8 nanostructures (e.g., nanoparticles,[25] and nanospheres [26]) and their

composites with carbons (Co_9S_8/reduced graphene oxides (RGO),[22] Co_9S_8/(N, S, P)-doped carbons,[27] Co_9S_8/Fe_3O_4/RGO[23] and Co_9S_8/MoS_2/Carbon fibres[25]) have been reported. For example, Co_9S_8/N,P-carbon powder nanocomposites prepared by molten-salt calcination method at 900 ^oC exhibited a HER overpotential of 261 mV at 10 mA cm^{-2} in alkaline medium.[20] N-Co_9S_8/Graphene nanocomposites was achieved with a OER Tafel slope of 82.7 mV Dec^{-1} and a overpotential of ~0.41 V at 10 mA cm^{-2} by a hydrothermal method.[22] In spite of enhanced electrocatalytic performance to some extent, the water splitting activity of the aforementioned Co_9S_8-based catalysts is still not satisfactory. One hand, the catalytic performance of powder Co_9S_8-based catalysts is greatly undermined because the active sites would be covered or annihilated during the preparation of test-electrode with polymer binders.[28] Moreover, powder-form materials are prone to detach from the surface of test-electrode at large working currents due to the bubble striking effect. This can greatly reduce life span and increase inner resistance. Additionally, numerous undesirable interfaces and extra resistance are inevitably introduced leading to higher overpotentials.[29] On the other hand, the synthetic condition for the Co_9S_8-base catalysts in these published works is always harsh with high temperature sintering and heavily polluted by using H_2S or organic precursors with sulfur sources (such as thiourea and trithiocyanuric acid). [30-32] In such a context, green and low-temperature sulfurization method must be established to fabricate high-activity binder-free Co_9S_8-base catalysts to achieve high performance.

In the present work, we report a simple and powerful sulfurization strategy to rationally design hollow $TiO_2@Co_9S_8$ core-branch arrays for the first time as robust bifunctional electrocatalysts for both OER and HER in alkaline medium. The bind-free $TiO_2@Co_9S_8$ core-branch arrays are proven with large porosity/surface area and strong adhesion on the conductive substrates, endowing them with more active cites, faster ions/electrons transport rate and better structural stability. Such unique structural features enable the $TiO_2@Co_9S_8$ core-branch arrays to deliver remarkably enhanced HER and OER properties compared to

pristine Co_9S_8 nanowires. Low overpotentials of 240 and 139 mV at 10 mA cm^{-2} as well as small Tafel slopes of 55 and 65 mV Dec^{-1} for OER and HER in alkaline medium are achieved by our TiO_2@Co_9S_8 core-branch electrode, respectively. More importantly, an advanced electrolysis cell with a highly low water splitting voltage of 1.56 V at 10 mA cm^{-2} and excellent durability (no any decay after soaking in the electrolyte for 10 days) is demonstrated when using the TiO_2@Co_9S_8 core-branch arrays as both cathode and anode, outperforming most of the developed electrochemical water splitting cells. Our novel electrode design/fabrication protocol can provide a reference for construction of high-performance integrated branch-core arrays for applications in electrocatalysis and energy storage.

2. Results and discussion

The TiO_2@Co_9S_8 hollow core-branch arrays are prepared via a low-temperature sulfurization on the preformed TiO_2@$Co_2(OH)_2CO_3$ core-shell arrays (**Figure S1**). Firstly, the $Co_2(OH)_2CO_3$ nanowire arrays on the nickel foam substrate are prepared by a simple hydrothermal synthesis. Apparently, the sample shows red color and homogeneous $Co_2(OH)_2CO_3$ nanowires of 80-100 nm are grown quasi-vertically onto the substrate (**Figure S2a-c**). These nanowires have a smooth surface and grow independently with non-interference, leaving a 3D porous structure. TEM images and selected area electron diffraction (SEAD) pattern demonstrate the smooth texture and single crystalline characteristics of the $Co_2(OH)_2CO_3$ nanowire (**Figure S2d-f**). The existence of $Co_2(OH)_2CO_3$ (JCPDS 48-0083) is supported by XRD and Raman analysis (**Figure S2g-h**). Then, a thin ALD-TiO_2 layer of ~10 nm is deposited on the $Co(OH)_2CO_3$ nanowires to form TiO_2@$Co(OH)_2CO_3$ core-shell nanowire arrays (**Figure S3a-e**). The color of sample turns into pale pink color (inset in **Figure S3a**). TEM and HRTEM images in **Figure S3d-f** clearly verify the core-shell structure and amorphous nature of the TiO_2 layer of ~10 nm. The co-existence of $Co_2(OH)_2CO_3$ and

TiO_2 is further verified by XRD and Raman analysis (**Figure S3g-h**). Finally, the hollow TiO_2@Co_9S_8 core-branch arrays are obtained after treating the TiO_2@$Co(OH)_2CO_3$ nanowires in 0.1M Na_2S solution at 90 ^oC for 9 h. After sulfurization, the color of sample turns to black due to the formation of Co_9S_8 (inset in **Figure 1a** and **Figure S4**). Interestingly, the previous dense core-shell structure of TiO_2@$Co(OH)_2CO_3$ disappears and perfect 3D hollow core-branch arrays architecture is successfully formed (**Figure 1b, c** and **S4a-c**). The internal TiO_2 nanotube core is uniformly decorated by the shell consisting of cross-linked Co_9S_8 nanoflakes with thicknesses of 10-15 nm. The diameter for the TiO_2@Co_9S_8 core-branch structure is about 400-450 nm. The diffraction rings of (400), (331) in SAED pattern (Inset in Figure 1c) and the measured layer spacing of about 0.30 nm corresponding to crystal planes of (311) indicate the existence of Co_9S_8 phase (**Figure 1d**). Energy dispersive X-ray (EDS) mapping images (**Figure 1e-f**) also indicate the presence and homogeneous distribution of Co, S, Ti and O elements in TiO_2@Co_9S_8 arrays samples, which further prove the hollow TiO_2 nanotube core and branch Co_9S_8 shell. It is noteworthy that the TiO_2 layer is vital to the formation of hollow TiO_2@Co_9S_8 core-branch architecture. Only common Co_9S_8 nanowire arrays are formed without the presence of TiO_2 layer (**Figure S5**). Furthermore, our present synthetic strategy is also versatile and powerful for growth on different substrates (e.g., carbon cloth, **Figure S6**). To reveal this sulfurization mechanism, it is inferred that there are two sulfurization pathways for the growth of Co_9S_8. In the presence of TiO_2 layer, the plausible reaction mechanism, most likely, is associated with the “oriented attachment” and “induced self-assembly” effects (**Figure S**7). It is known that the Na_2S solution hydrolyzes and produces acid species (e.g., HS-, H_2S, etc.), which can react with the basic $Co_2(OH)_2CO_3$. The reactants with S sources are prone to preconcentrate along the outer surface of the TiO_2 layer. In the meantime, the dissolved Co cations transport

outwards to meet the S sources to form Co_9S_8 crystals leading to the disappearance of $Co_2(OH)_2CO_3$ nanowire. Here the TiO_2 layer acts as the backbone for heterogeneous nucleation and guides the preferential growth of Co_9S_8. This process is believed to be involved with spontaneous "oriented attachment" and "induced self-assembly" of adjacent Co_9S_8 particles when supersaturated solution with considerable Co_9S_8 crystals are formed. The Co_9S_8 crystals are attached to the surface of TiO_2 layer to generate active nucleation centers, which would minimize the interfacial energy barrier for the subsequent growth of Co_9S_8. Finally, these Co_9S_8 crystals self-assemble with each other resulting in the formation of TiO_2@Co_9S_8 hollow core-branch arrays. On the other hand, without the TiO_2 layer, the direct conversion would take place and produce common Co_9S_8 nanowire arrays.

To further highlight the benefits of core-branch hollow arrays, the specific surface area was measured by BET analysis (**Figure S8**). The pristine Co_9S_8 nanowire arrays and TiO_2@Co_9S_8 core-branch arrays grown on the nickel foam substrate exhibit a specific surface area of 1.4 and 4.0 $m^2\ g^{-1}$, respectively, indicating that the design of hollow core-branch structure can greatly increase the surface area. Noteworthy that the nickel foam substrate accounts for about 88 % and 83 % in the weight of nickel foam supported TiO_2@Co_9S_8 and Co_9S_8 nanowire samples, respectively. As a result, the specific surface area of the individual TiO_2@Co_9S_8 is estimated to be ~33.4 $m^2\ g^{-1}$ excluding the nickel foam, far ahead of the Co_9S_8 nanowire samples (~8 $m^2\ g^{-1}$). It suggests that the core-branch structure is favorable for providing more active area/sites exposed and improve the utilization of active Co_9S_8 catalysts.

X-ray photoelectron spectroscopy (XPS) and Raman tests were performed to further determine the phase and composition. For the TiO_2@Co_9S_8 arrays, the XPS survey spectrum verifies the presence of Co, S, Ti and O elements (**Figure 2a**), consistent with the analysis of EDS mapping above. Only Co, S, and O element exist in the Co_9S_8 nanowire arrays. The O element in Co_9S_8 nanowire sample may be from OH^-.[33] **Figure 2b** shows the high-resolution

S 2p spectra of both samples. Two core levels (S 2p3/2 and S 2p1/2) are located at 161.3 and 163.1 eV, respectively, which match well with the electronic states of Co_9S_8. The high-resolution Co 2p spectra of both samples possess typical core levels of Co 2p1/2 (796.5 eV) and Co 2p3/2 (780.7 eV) and two satellite peaks (**Figure 2c**).[33-35] Meanwhile, the presence of TiO_2 in the TiO_2@Co_9S_8 arrays is also supported by Ti 2p and O1s spectra (**Figure S9**). The above results are strongly supported by Raman analysis (**Figure 2d**). Five characteristic peaks of Co_9S_8 phase (218, 253, 316, 373 and 685 cm^{-1}) are found in both samples. Moreover, the TiO_2@Co_9S_8 sample has a new peak at 150 cm^{-1}, revealing the existence of TiO_2.[36] All these results mutually support that TiO_2@Co_9S_8 and Co_9S_8 nanowire arrays are successfully fabricated via our facile sulfurization method.

The electrochemical application of TiO_2@Co_9S_8 arrays as electrocatalysts for water splitting are thoroughly characterized. First, the electrochemical OER activities of the samples were investigated by using a simple three-electrode system in 1 M KOH solution. In our experiment, four different electrodes ($Co_2(OH)_2CO_3$ nanowire arrays, TiO_2@$Co_2(OH)_2CO_3$ core-shell arrays, Co_9S_8 nanowire arrays, and TiO_2@Co_9S_8 core-branch arrays) are selected for OER comparison. **Figure 3a** presents the linear sweep voltammetry (LSV) curves of these four different electrodes. Significantly, the TiO_2@Co_9S_8 electrode exhibits the best OER catalytic performance with the lowest overpotential (240 mV at the current density of 10 mA cm^{-2}), superior to the Co_9S_8 (276 mV), $Co_2(OH)_2CO_3$ (330 mV) and TiO_2@$Co_2(OH)_2CO_3$ (350 mV) electrodes. The present overpotential is also substantially lower than recently reported Co_9S_8-based catalysts at the same current density, such as Co_9S_8@N and S co-doped porous carbon tube (310 mV),[27] hollow Co_9S_8 microplates (273 mV)[26] and Fe_3O_4@Co_9S_8/rGO (340 mV).[27] This indicates the construction of hollow core-branch architecture is favorable for the reinforcement of OER, further proven by the Tafel slope analysis (**Figure 3b**). The TiO_2@Co_9S_8 electrode exhibits the lowest of Tafel slope of 55 mV dec^{-1}, much better than other counterparts, suggesting its fastest OER process (**Table S**1). To

deepen the understanding of the enhanced OER activity, the effective electrochemical active surface area (ECSA) of all samples was estimated by testing the double-layer capacitance (DLC) according to the CV results at different scan rates (**Figure S10**).[37] The obtained current density is plotted as a function with scan rates in Figure 3c. The ECSA value is linearly proportional to the DLC value, equaling to the half of the slope value. Remarkably, the highest capacitance up to 48 mF cm^{-2} is achieved by the $TiO_2@Co_9S_8$ electrode, demonstrating its largest ECSA, much larger than the $Co_2(OH)_2CO_3$ (28 mF cm^{-2}), $TiO_2@Co_2(OH)_2CO_3$ (11 mF cm^{-2}) and Co_9S_8 (34 mF cm^{-2}) electrodes, indicating the markedly improved active areas for the $TiO_2@Co_9S_8$ electrode. Furthermore, as presented in **Figure 3d**, the smallest circle diameter of the $TiO_2@Co_9S_8$ electrode show that it possesses the lowest charge transfer resistance (R_{ct}), revealing that the $TiO_2@Co_9S_8$ electrode has faster electrocatalytic reaction kinetics. The unique design of hollow core-branch arrays provides positive effects in the enhancement of OER performance. 1) Direct growth of $TiO_2@Co_9S_8$ arrays on conductive substrates avoids the use of insulated polymer binders and annihilation of active sites. 2) The cross-linked Co_9S_8 nanoflakes with large specific surface area increase accessible area between active materials and electrolyte, and provide more active sites. Moreover, the hollow core can serve as buffer “electrolyte reservoirs” to accelerate the transport of ions leading to faster catalytic reactions. In addition, the porous and hollow structure is beneficial for overflow of O_2 and will not block the active sites during water splitting processes. Noticeably, the $TiO_2@Co_9S_8$ core-branch electrode also possesses excellent long-term OER durability. As shown in **Figure 3e**, the $TiO_2@Co_9S_8$ electrode retains higher activity and more stable life span than the Co_9S_8 nanowire electrode at different current densities ranging from 10 to 50 mA cm^{-2}.

Apart from excellent OER activity, the obtained $TiO_2@Co_9S_8$ electrode also exhibits outstanding HER catalytic performance in alkaline solution. As shown in **Figure 4a**, the $TiO_2@Co_9S_8$ electrode presents a remarkably low overpotential of 139 mV at 10 mA cm^{-2},

superior to the Co_9S_8 (222 mV), $Co_2(OH)_2CO_3$ (197 mV) and $TiO_2@Co_2(OH)_2CO_3$ (226 mV) electrodes. Moreover, the $TiO_2@Co_9S_8$ electrode displays the lowest Tafel slopes (65 mV Dec^{-1}), better than the $Co_2(OH)_2CO_3$ (102 mV Dec^{-1}), $TiO_2@Co_2(OH)_2CO_3$ (126 mV Dec^{-1}), Co_9S_8 electrodes (85 mV Dec^{-1}) (**Figure 4b**) as well as other electrocatalysts (**Table S1**). Also, long-term HER durability is demonstrated for the $TiO_2@Co_9S_8$ electrode at different current densities (**Figure 4c**). It is justified that our designed hollow core-branch array architecture can promote the HER activity of Co_9S_8.

Due to the prominent activities for both OER and HER, the $TiO_2@Co_9S_8$ electrode could be utilized as an efficient bifunctional electrocatalyst for overall water splitting in alkaline medium. **Figure 5a** shows the overall water splitting activity of two-electrode system with the $TiO_2@Co_9S_8$ electrocatalysts as both cathode and anode in 1 M KOH solution (denoted as $TiO_2@Co_9S_8||TiO_2@Co_9S_8$). Impressively, a significantly low cell voltage of 1.56 V is obtained at the current density of 10 mA cm^{-2} (**Figure 5a**), substantially lower than the Co_9S_8 || Co_9S_8 catalyzer cell (1.71 V) and other reported bifunctional electrocatalysts,[6, 16, 27, 38-46] such as Co_3O_4 (1.63 V), $NiCo_2O_4$ (1.72 V), CoO (1.63 V), NiP (1.63 V), Co_9S_8 (1.6 V) (Figure 5b) and even ~~lower than~~ close to the Pt/C || IrO_2 (1.54 V) catalyzer cell.[44] **Figure 5c** compares the chronopotentiometry curves of the $TiO_2@Co_9S_8$ || $TiO_2@Co_9S_8$ and Co_9S_8 || Co_9S_8 catalyzer cells collected at 10 mA cm^{-2}. The $TiO_2@Co_9S_8$ || $TiO_2@Co_9S_8$ catalyzer cell shows higher activity with lower overpotential for overall water splitting, demonstrating its long-term durability with no decay after 30 h. In addition, continuous hydrogen and oxygen bubbles could be noticed on the anode and cathode during the stability test, respectively (Inset in **Figure 5c**). SEM and TEM images reveal that the uniform hollow core-branch arrays structure is still well preserved after 30 h (**Figure S11**), demonstrating the excellent structural stability of the $TiO_2@Co_9S_8$ electrode. This is mainly due to the high mechanical strength of TiO_2 core and good adhesion between TiO_2 and Co_9S_8 nanoflakes. In addition, in order to meet practical application, the LSV performance is performed after soaking the $TiO_2@Co_9S_8$

electrode in the electrolyte for 10 days (when current is not flowing). Impressively, the whole performance is very stable and water splitting voltage does not show any decay. All the above results indicate that this core-branch hollow structure would remarkably improve electrochemical activities for OER/HER. This makes the $TiO_2@Co_9S_8$ hollow core-branch arrays promising catalysts for practical application in alkaline water splitting.

3. Conclusions

In summary, we have demonstrated a facile and high-efficiency sulfurization approach to realize the rational synthesis of hollow $TiO_2@Co_9S_8$ core-branch arrays as robust bifunctional electrocatalysts for both OER and HER in alkaline. Cross-linked Co_9S_8 nanoflakes are uniformly assembled on the hollow TiO_2 core forming free-standing arrays. Meanwhile, the proposed synthetic method is versatile and applicable to different conductive substrates and core-branch morphology. Due to enhanced surface area & porosity, and binder-free adhesion with the conductive substrate, the designed $TiO_2@Co_9S_8$ arrays are utilized as bifunctional catalysts for OER/HER and proven with excellent performances with low Tafel slopes & overpotentials and superior cycling stability. Moreover, a low voltage (~1.56 V) for overall water splitting is achieved in the $TiO_2@Co_9S_8$ || $TiO_2@Co_9S_8$ catalyzer cell, superior to other metal sulfides/oxides in the literature. Our work opens a new door to construct advanced electrocatalysts based on novel hollow core-branch array architecture.

Experimental

Preparation of $TiO_2@Co_9S_8$ core-branch arrays. Uniform $Co_2(OH)_2CO_3$ nanowires arrays were prepared by a simple hydrothermal method. First, 0.75g $Co(NO_3)_2$, 0.25g NH_4F and 0.75g $CO(NH_2)_2$ were dissolved in 75 mL deionized water to form hydrothermal solution. Then the above solution was transferred into a Teflon-linked steel autoclave, which was kept at 120 ^oC for 6 h. After naturally cooling, the $Co_2(OH)_2CO_3$ nanowires arrays were rinsed by

deionized water. Then, the above $Co_2(OH)_2CO_3$ nanowire arrays were coated with a layer of TiO_2 (~10 nm) by atomic layer deposition (ALD Beneq TFS 200) with $TiCl_4$ and H_2O as the Ti and O precursors at 120 ^oC for 140 cycles. Then, in a typical sulfurization process, the above TiO_2@$Co(OH)_2CO_3$ nanowires arrays were immersed into 0.1M Na_2S solution and kept at 90 ^oC for 9 h. After naturally cooling, the obtained TiO_2@Co_9S_8 core-branch arrays were rinsed by deionized water. For comparison, the Co_9S_8 nanowires arrays were prepared by a direct sulfurization procedure for $Co_2(OH)_2CO_3$ nanowires arrays as the same sulfurization parameters above.

Material characterization. Morphologies and microstructures of all samples were characterized by using a field emission scanning electron microscope (FESEM, Hitachi SU8010) and the transmission electron microscope (TEM, JEOL 2100F). Specific surface areas distributions were characterized by using Porosity Instruments (BET, JW-BK112). The crystal structure of all samples by using X-ray diffraction (XRD) reactor with Cu Ka radiation (RigakuD/Max-2550). Raman spectra was obtained by using RenishawinVia Raman microscopy under 514nm laser excitation. X-Ray photoelectron spectroscopy was tested by using an Al Ka source with an ESCALAB_250Xi X-Ray photoelectron spectrometer.

Electrochemical characterizations. OER and HER performances of all samples were performed by using an electrochemical workstation (CH Instrument 660D) with a standard three-electrode setup at room temperature, where carbon rod (D = 8 mm) and saturated calomel electrode (SCE) were used as the counter electrode and reference electrode, respectively. The as-prepared samples were used as the working electrode. The electrolyte of electrochemical tests was 1 M KOH solution. All potentials in this manuscript are referred to the RHE. The conversion of potential between E(RHE) and E(SCE) obeys the following equation: E(RHE) = E(SCE) + 1.0714 V. All samples were first performed the CV test at 50 mV s^{-1} to stabilize the current. The linear sweep voltammetry (LSV) tests were performed at a scan rate of 5 mV s^{-1}. The Tafel plots were derived from LSV curves with a scan rate of 1

mV s^{-1}. The electrochemical impedance spectroscopy (EIS) were conducted at the polarization voltage corresponding to current density of 10 mA cm^{-2}, in a frequency range from 100 kHz to 50 mHz with an AC amplitude of 10 mV. The stability test was carried out at different constant current densities (10, 30, and 50 mA cm^{-2}) for 10 h each. All these results were obtained by iR-compensation. Overall water splitting was performed in a two-electrode catalyzer for 30 h at 10 mA cm^{-2}, where two TiO_2@Co_9S_8 electrodes with the same geometric area were used as the catalysts for OER and HER, respectively.

Supporting Information

Supporting Information is available from the Wiley Online Library or from the author.

Acknowledgements

This work is supported by National Natural Science Foundation of China (Grant No. 51728204, 51772272 and 51502263), Qianjiang Talents Plan D (QJD1602029), Program for Innovative Research Team in University of Ministry of Education of China (IRT13037), Startup Foundation for Hundred-Talent Program of Zhejiang University, the Fundamental Research Funds for the Central Universities (2015XZZX010-02), Guangdong Natural Science Funds for Distinguished Young Scholar (2014A030306048), and Pearl River S&T Nova Program of Guangzhou (201610010080).

Received: ((will be filled in by the editorial staff))
Revised: ((will be filled in by the editorial staff))
Published online: ((will be filled in by the editorial staff))

References

[1] M. Dresselhaus, I. Thomas, Nature 2001, 414, 332.

[2] Y. Shang, L. Guo, Adv. Sci. 2015, 2, 1500140.

[3] W. Wang, X. M. Xu, W. Zhou, Z. P. Shao, Adv. Sci. 2017, 4, 1600371.

[4] S. Deng, Y. Zhong, Y. Zeng, Y. Wang, Z. Yao, F. Yang, S. Lin, X. Wang, X. Lu, X. Xia, Adv. Mater. 2017, 29, 1700748.

[5] Z. L. Zhang, Y. R. Fang, W. H. Wang, L. Chen, M. T. Sun, Adv. Sci. 2016, 3, 1500215.

[6] Y. Liu, Q. Li, R. Si, G. D. Li, W. Li, D. P. Liu, D. Wang, L. Sun, Y. Zhang, X. Zou, Adv. Mater. 2017, 29, 1606200.

[7] S. Jin, N. Li, H. Cui, C. Wang, Nano Energy 2013, 2, 1128.

[8] Y. Li, P. Hasin, Y. Wu, Adv. Mater. 2010, 22, 1926.

[9] J. X. Feng, S. H. Ye, H. Xu, Y. X. Tong, G. R. Li, Advanced Materials 2016, 28, 4698.

[10] Y. Yan, B. Xia, B. Zhao, X. Wang, J. Mater. Chem.A 2016, 4, 17587

[11] X. Duan, J. Xu, Z. Wei, J. Ma, S. Guo, H. Liu, S. Dou, Small Methods 2017, 1700156.

[12] L. Wang, C. Yang, S. Dou, S. Wang, J. Zhang, X. Gao, J. Ma, Y. Yu, Electrochim. Acta 2016, 219, 592.

[13] J. Zhang, T. Wang, P. Liu, Z. Liao, S. Liu, X. Zhuang, M. Chen, E. Zschech, X. Feng, Nat. Commun. 2017, 8, 15473.

[14] J. Zhang, T. Wang, P. Liu, S. Liu, R. Dong, X. Zhuang, M. Chen, X. Feng, Energy Environ. Sci. 2016, 9, 2789.

[15] J. Zhang, T. Wang, D. Pohl, B. Rellinghaus, R. Dong, S. Liu, X. Zhuang, X. Feng, Angewandte Chemie 2016, 128, 6814.

[16] Z. Peng, D. Jia, A. M. Al-Enizi, A. A. Elzatahry, G. Zheng, Adv. Energy Mater. 2015, 5, 1402031.

[17] D. Kong, H. Wang, Z. Lu, Y. Cui, J. Am. Chem. Soc. 2014, 136, 4897.

[18] E. J. Popczun, J. R. McKone, C. G. Read, A. J. Biacchi, A. M. Wiltrout, N. S. Lewis, R. E. Schaak, J. Am. Chem. Soc. 2013, 135, 9267.

[19] B. Cao, G. M. Veith, J. C. Neuefeind, R. R. Adzic, P. G. Khalifah, J. Am. Chem. Soc. 2013, 135, 19186.

[20]R. Liu, H. Zhang, X. Zhang, T. Wu, H. Zhao, G. Wang, RSC Adv. 2017, 7, 19181.

[21]X. Cao, X. Zheng, J. Tian, C. Jin, K. Ke, R. Yang, Electrochim. Acta 2016, 191, 776.

[22]S. Dou, L. Tao, J. Huo, S. Wang, L. Dai, Energy Environ. Sci. 2016, 9, 1320.

[23]J. Yang, G. Zhu, Y. Liu, J. Xia, Z. Ji, X. Shen, S. Wu, Adv. Funct. Mater. 2016, 26, 4712.

[24]H. Zhu, J. Zhang, R. Yanzhang, M. Du, Q. Wang, G. Gao, J. Wu, G. Wu, M. Zhang, B. Liu, Adv. Mater. 2015, 27, 4752.

[25]X. Zhou, X. Yang, M. N. Hedhili, H. Li, S. Min, J. Ming, K.-W. Huang, W. Zhang, L.-J. Li, Nano Energy 2017, 32, 470.

[26]H. Liu, F.-X. Ma, C.-Y. Xu, L. Yang, Y. Du, P.-P. Wang, S. Yang, L. Zhen, ACS Appl. Mater. Interfaces 2017, 9, 11634.

[27]S. Huang, Y. Meng, S. He, A. Goswami, Q. Wu, J. Li, S. Tong, T. Asefa, M. Wu, Adv. Funct. Mater. 2017, 27, 1606585.

[28]S. Anantharaj, S. R. Ede, K. Sakthikumar, K. Karthick, S. Mishra, S. Kundu, ACS Catalysis 2016, 6, 8069.

[29]M.-S. Balogun, Y. Huang, W. Qiu, H. Yang, H. Ji, Y. Tong, Materials Today 2017, 20, 425.

[30]L.-L. Feng, G.-D. Li, Y. Liu, Y. Wu, H. Chen, Y. Wang, Y.-C. Zou, D. Wang, X. Zou, ACS Appl. Mater. Interfaces 2015, 7, 980.

[31]Y. Tang, F. Jing, Z. Xu, F. Zhang, Y. Mai, D. Wu, ACS Appl. Mater. Interfaces 2017, 9, 12340.

[32]Y. Pan, Y. Liu, C. Liu, Appl. Surf. Sci. 2015, 357, 1133.

[33]X.-h. Xia, J.-p. Tu, Y.-q. Zhang, Y.-j. Mai, X.-l. Wang, C.-d. Gu, X.-b. Zhao, RSC Adv. 2012, 2, 1835.

[34]J. A. Vigil, T. N. Lambert, B. T. Christensen, J. Mater. Chem.A 2016, 4, 7549.

[35]L.-L. Feng, M. Fan, Y. Wu, Y. Liu, G.-D. Li, H. Chen, W. Chen, D. Wang, X. Zou, J. Mater. Chem.A 2016, 4, 6860.

[36]W. Zhang, Y. He, M. Zhang, Z. Yin, Q. Chen, J. Phys. D: Appl. Phys. 2000, 33, 912.

[37]Y. Zhang, B. Ouyang, J. Xu, S. Chen, R. S. Rawat, H. J. Fan, Adv. Energy Mater. 2016, 6, 1600221.

[38]Y. P. Zhu, T. Y. Ma, M. Jaroniec, S. Z. Qiao, Angew. Chem. Int. Ed. 2017, 56, 1324.

[39]H. Wang, H.-W. Lee, Y. Deng, Z. Lu, P.-C. Hsu, Y. Liu, D. Lin, Y. Cui, Nat. Commun. 2015, 6, 7261.

[40]L.-A. Stern, L. Feng, F. Song, X. Hu, Energy Environ. Sci. 2015, 8, 2347.

[41]C. Tang, N. Cheng, Z. Pu, W. Xing, X. Sun, Angew. Chem. Int. Ed. 2015, 127, 9483.

[42]H. Liang, L. Li, F. Meng, L. Dang, J. Zhuo, A. Forticaux, Z. Wang, S. Jin, Chem. Mater. 2015, 27, 5702.

[43]J. Li, Y. Wang, T. Zhou, H. Zhang, X. Sun, J. Tang, L. Zhang, A. M. Al-Enizi, Z. Yang, G. Zheng, J. Am. Chem. Soc 2015, 137, 14305.

[44]N. Jiang, B. You, M. Sheng, Y. Sun, Angew. Chem. Int. Ed. 2015, 127, 6349.

[45]Y. P. Zhu, Y. P. Liu, T. Z. Ren, Z. Y. Yuan, Adv. Funct. Mater. 2015, 25, 7337.

[46]M. Ledendecker, S. Krick Calderón, C. Papp, H. P. Steinrück, M. Antonietti, M. Shalom, Angew. Chem. Int. Ed. 2015, 127, 12538.

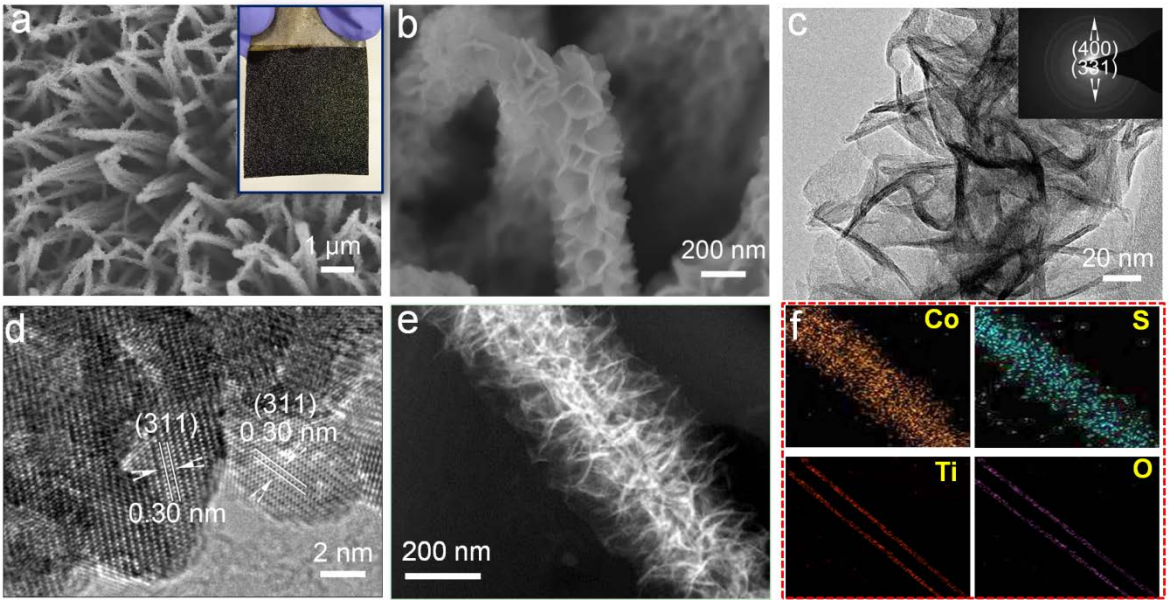

Figure 1. (a, b) SEM images (Optical photo in inset); (c) TEM image (SAED pattern in inset); (d) HRTEM image; (e) high-angle annular dark-field STEM image and (f) EDS elemental mapping images of Co, S, Ti and O of the TiO_2@Co_9S_8 hollow core-branch arrays.

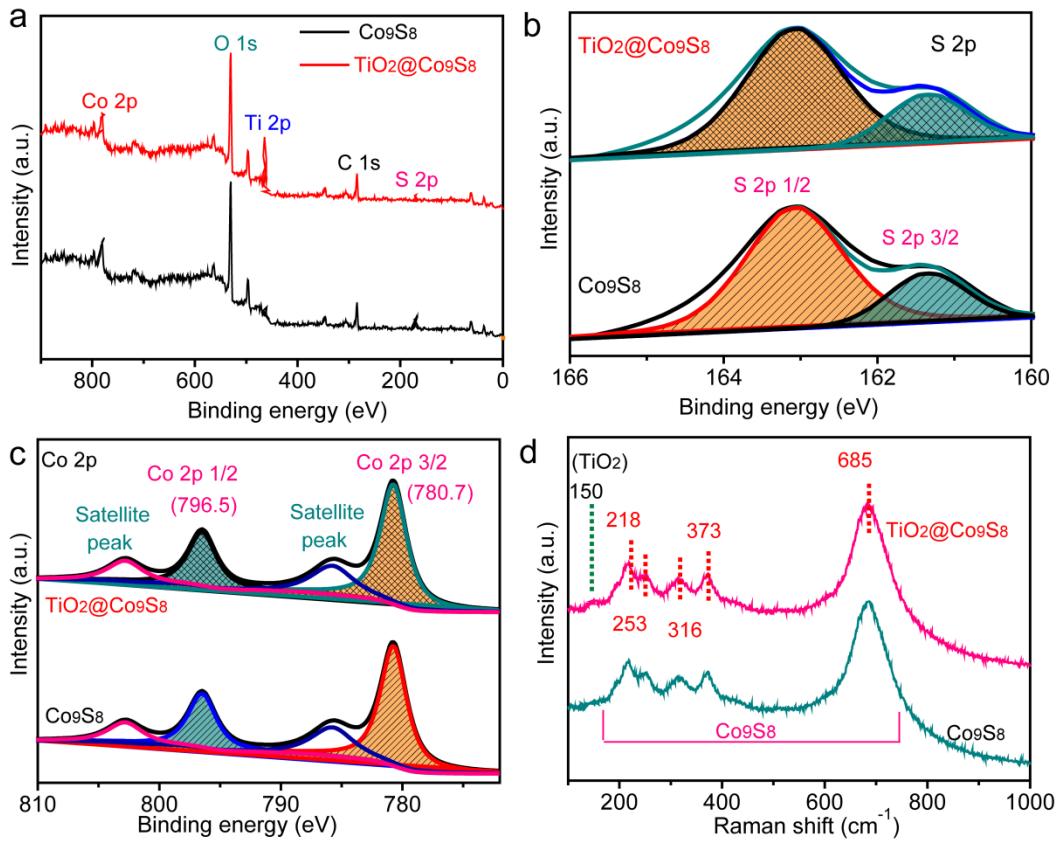

Figure 2. XPS and Raman characterizations of TiO_2@Co_9S_8 and Co_9S_8 arrays: (a) XPS survey spectra; (b) core-level S 2p XPS spectra; (c) core-level Co 2p XPS spectra and (d) Raman spectra of the Co_9S_8 and TiO_2@Co_9S_8 arrays.

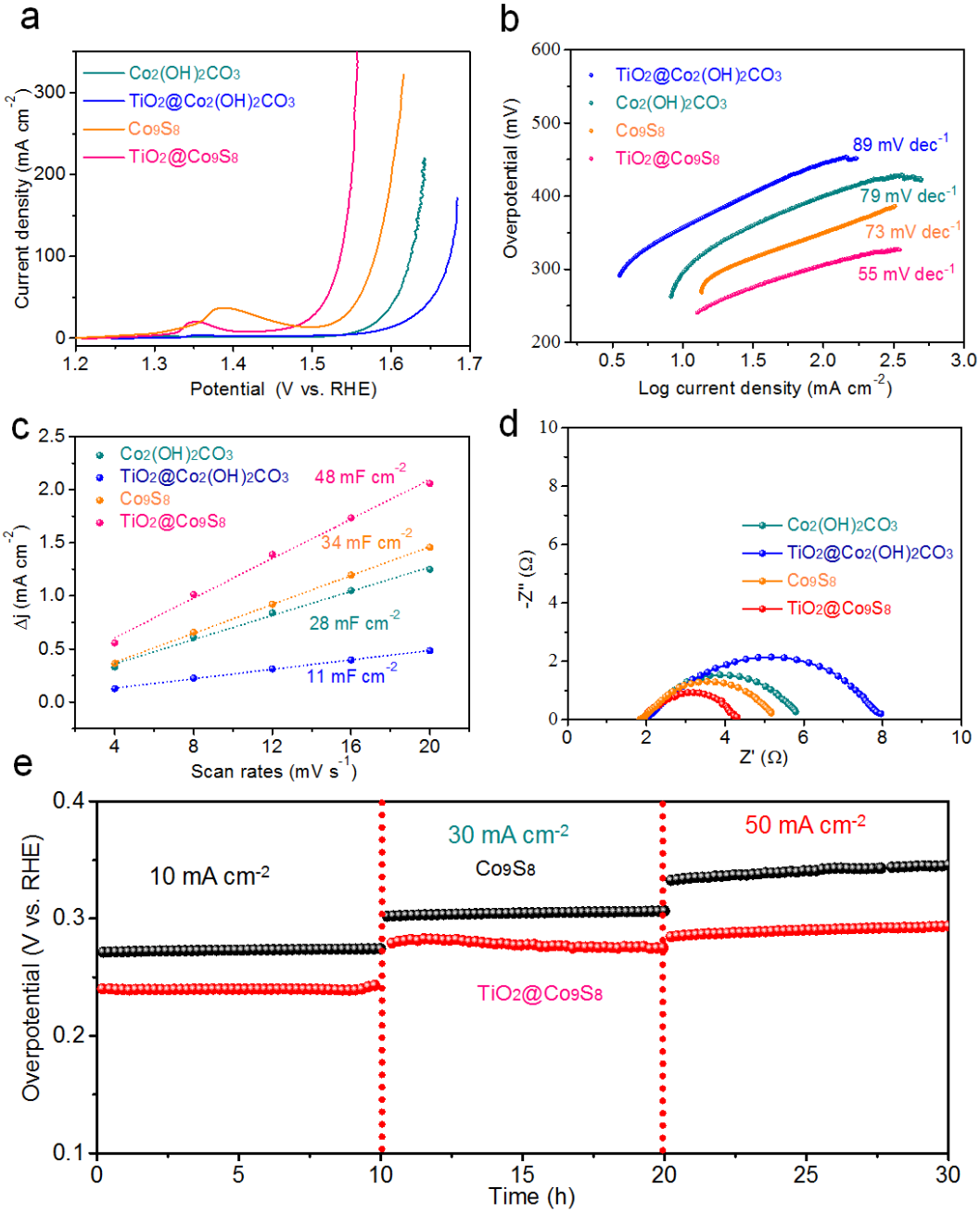

Figure 3. OER performances: (a) LSV curves at 5 mV s^{-1}; (b) Tafel plots; (c) The ratio of current density with various scan rates and (d) Nyquist plots of $Co_2(OH)_2CO_3$, $TiO_2@Co_2(OH)_2CO_3$, Co_9S_8 and $TiO_2@Co_9S_8$ electrodes; (e) Electrochemical stability of the Co_9S_8 and $TiO_2@Co_9S_8$ electrodes at different current densities.

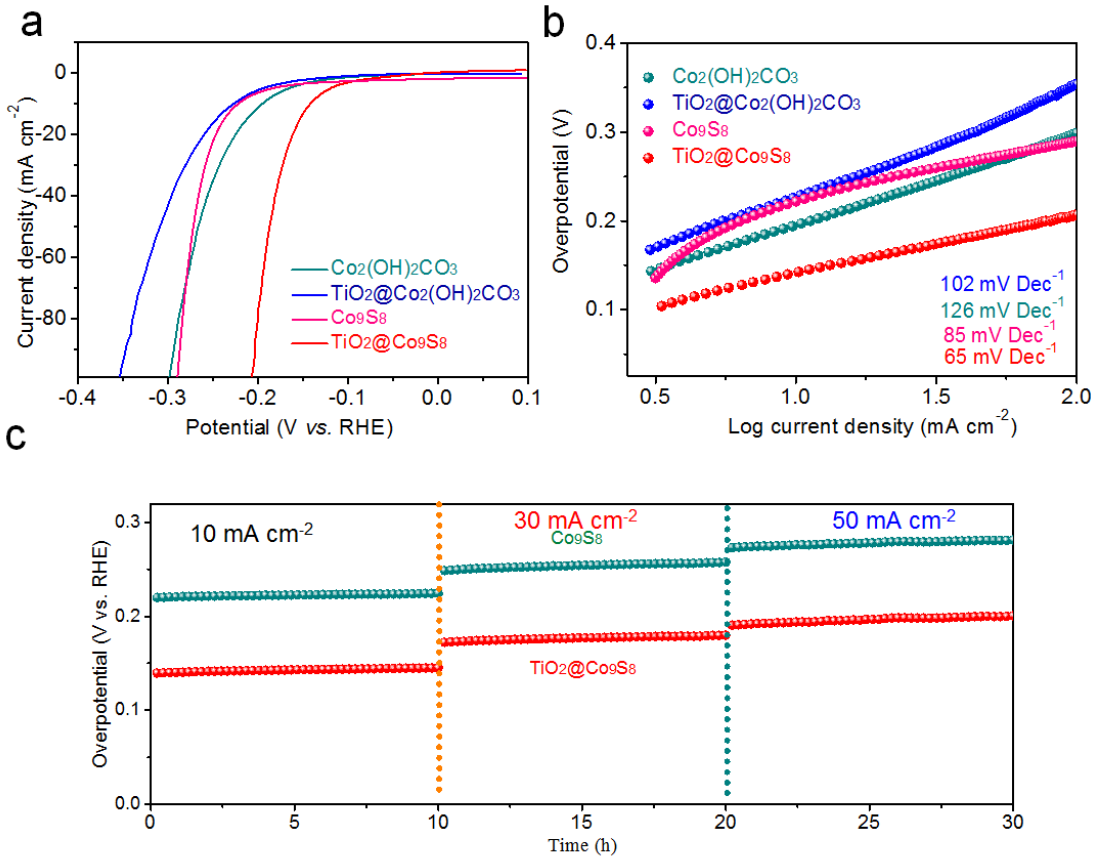

Figure 4. HER performances: (a) LSV curves at 5 mV s^{-1}; (b) Tafel plots of $Co_2(OH)_2CO_3$, $TiO_2@Co_2(OH)_2CO_3$, Co_9S_8 and $TiO_2@Co_9S_8$ electrodes, and (c) Electrochemical stability of the Co_9S_8 and $TiO_2@Co_9S_8$ electrodes at different current densities and times.

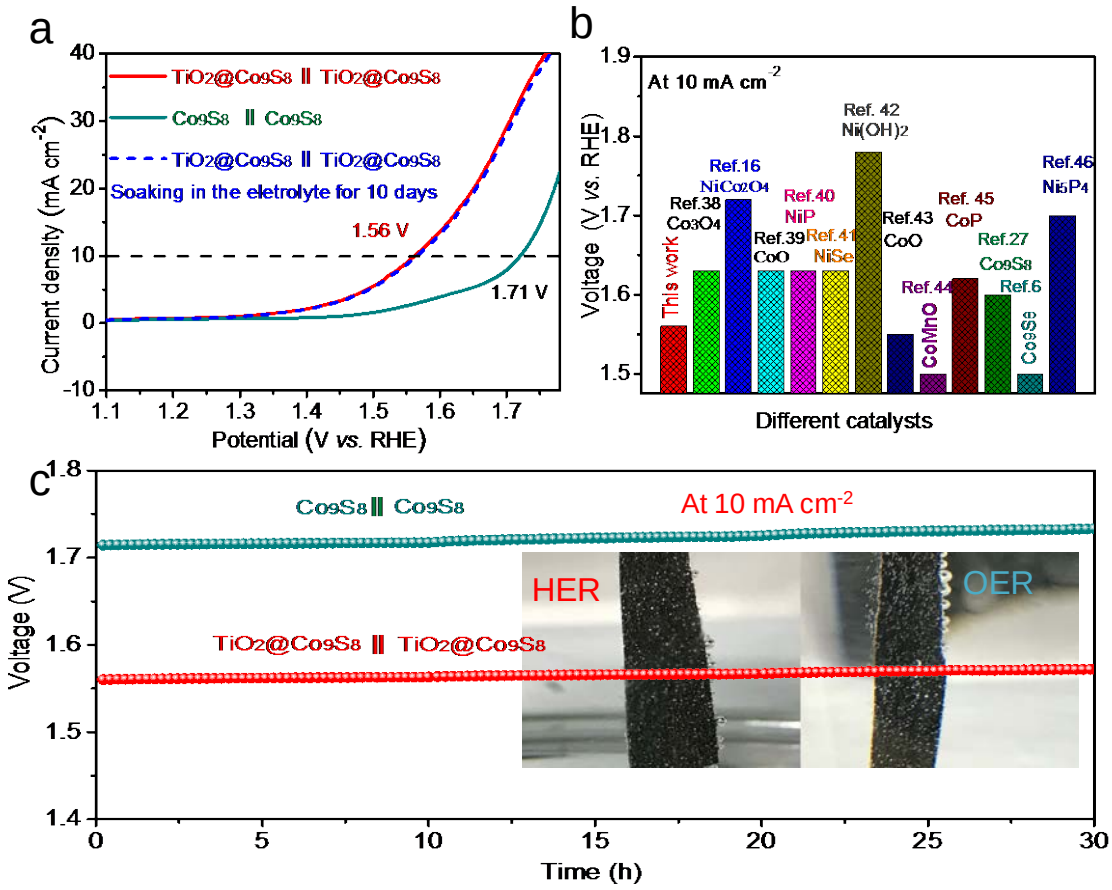

Figure 5. Overall water splitting performance of electrolysis cells: $TiO_2@Co_9S_8$‖ $TiO_2@Co_9S_8$ and Co_9S_8‖Co_9S_8. (a) LSV curves; (b) Comparison of overall water splitting performance between $TiO_2@Co_9S_8$‖$TiO_2@Co_9S_8$ and other electrocatalysts in the literature, and (c) Electrochemical stability at 10 mA cm^{-2}.

A new kind of binder-free hollow $TiO_2@Co_9S_8$ core-branch arrays are developed as highly active OER and HER electrocatalysts for the first time by a facile and powerful sulfurization strategy. The as-obtained $TiO_2@Co_9S_8$ electrode exceptional electrocatalytic performance, with low overpotentials of 240 and 139 mV at 10 mA cm^{-2} as well as low Tafel slopes of 55 and 65 Dec^{-1} for OER and HER in alkaline medium, respectively. Moreover, a remarkable low voltage of 1.56 V for overall water splitting is achieved based on the $TiO_2@Co_9S_8$ arrays as both cathode and anode, superior to most of other metal sulfides/oxides.

Keywords: cobalt sulfide; arrays; electrochemical water splitting; hydrogen evolution reaction; oxygen evolution reaction;

S. J. Deng, Y. Zhong, Y. X. Zeng, Y. D. Wang, X. L. Wang, X. H. Lu*, X. H. Xia*, and J. P. Tu

Hollow $TiO_2@Co_9S_8$ Core-Branch Arrays as Bifunctional Electrocatalysts for Efficient Oxygen/Hydrogen Production

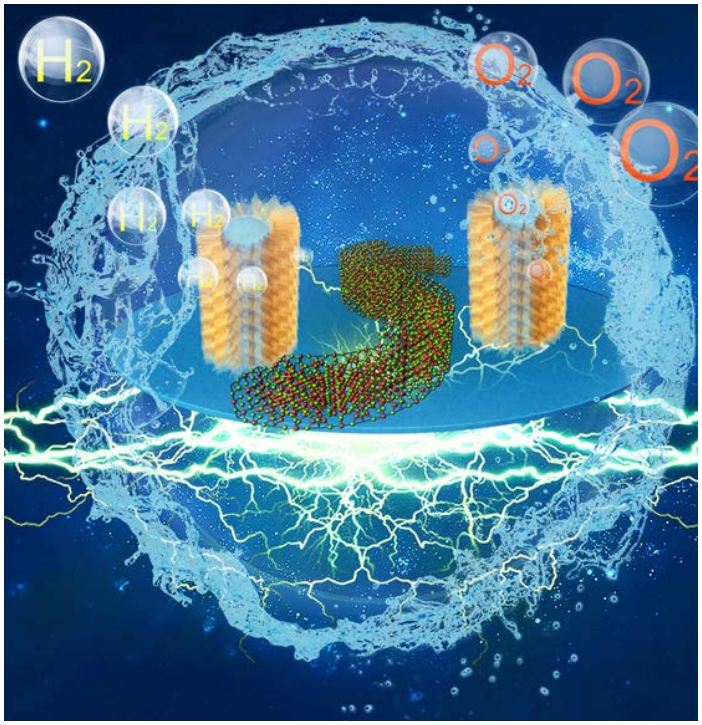

((Supporting Information can be included here using this template))

Supporting Information

Hollow TiO_2@Co_9S_8 Core-Branch Arrays as Bifunctional Electrocatalysts for Efficient Oxygen/Hydrogen Production

Shengjue Deng[1], *Yu Zhong*[1], *Yinxiang Zeng*[2], *Yadong Wang*[3], *Xiuli Wang*[1], *Xihong Lu*[2]*, *Xinhui Xia*[1]*, *Jiangping Tu*[1]

[1] *State Key Laboratory of Silicon Materials, Key Laboratory of Advanced Materials and Applications for Batteries of Zhejiang Province, and Department of Materials Science and Engineering, Zhejiang University, Hangzhou 310027, P. R. China.*

[2] *MOE of the Key Laboratory of Bioinorganic and Synthetic Chemistry, KLGHEI of Environment and Energy Chemistry, School of Chemistry, Sun Yat-Sen University, Guangzhou 510275, China.*

[3] *School of Engineering, Nanyang Polytechnic, 569830, Singapore*

Correspondence and requests for materials should be addressed to X. Xia (email: helloxxh@zju.edu.cn) and X. Lu (email: luxh6@mail.sysu.edu.cn)

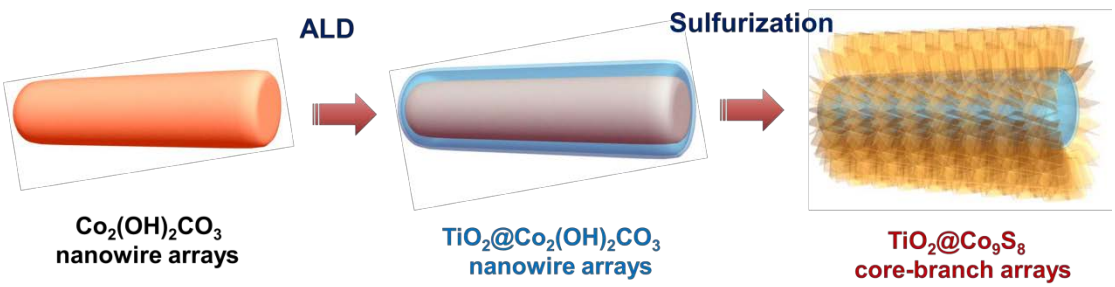

Figure S1. Growth schematics of TiO_2@Co_9S_8 hollow core-branch arrays.

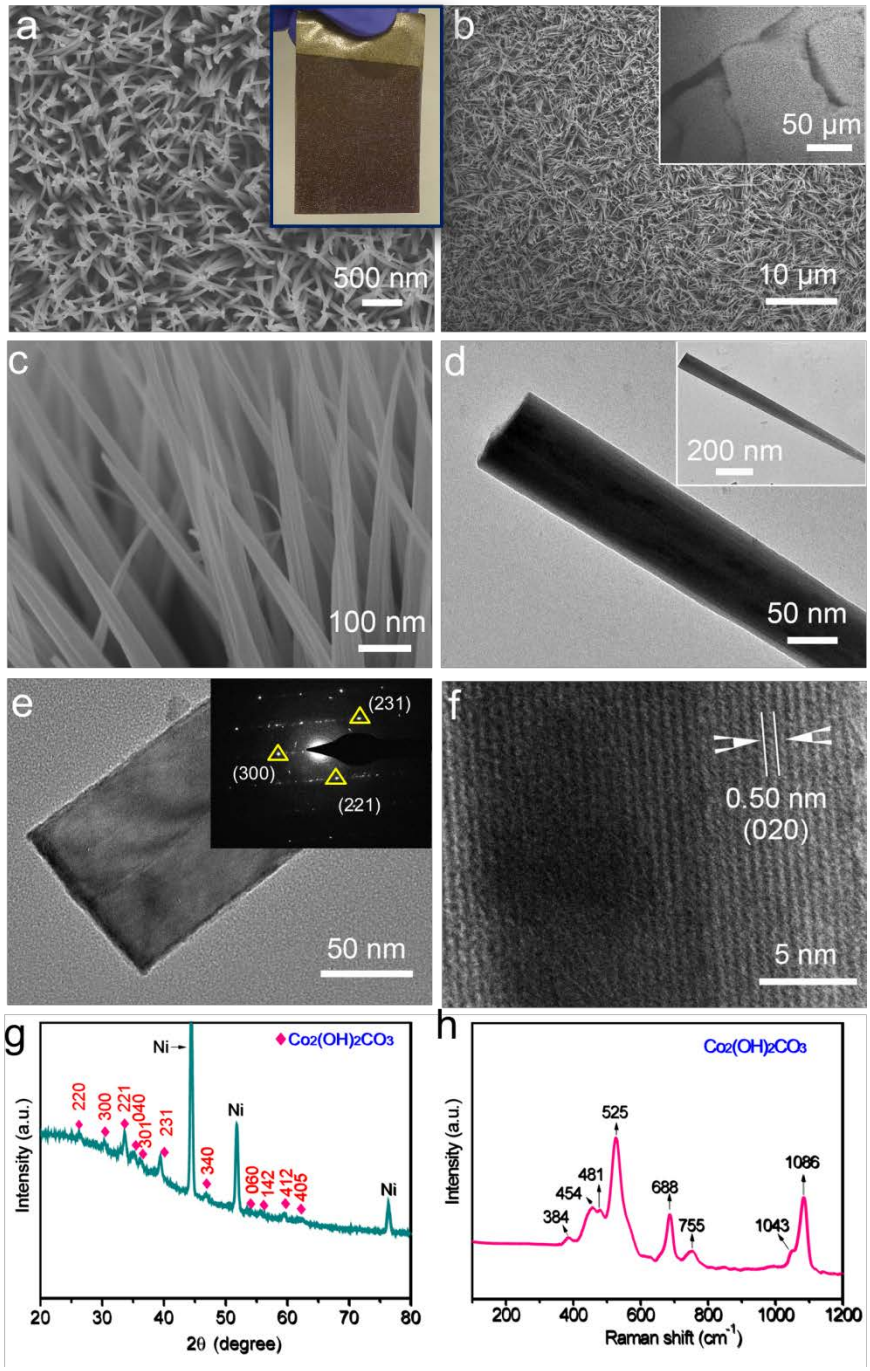

Figure S2. Morphology and microstructure characterizations of $Co_2(OH)_2CO_3$ nanowires arrays: (a-c) SEM images (photo of sample in inset); (d-f) TEM-HRTEM images (SAED pattern in inset); (g) XRD pattern; (h) Raman spectrum.

Except for the peaks of nickel foam substrate, the left diffraction peaks are indexed well with the crystal planes of $Co_2(OH)_2CO_3$ (JCPDS 48-0083) (**Figure S2**g), indicating the formation of high crystallinity of $Co_2(OH)_2CO_3$. Its Raman spectrum (**Figure S2**h) shows eight typical peaks of $Co_2(OH)_2CO_3$ in the region of 200-1100 cm^{-1}.

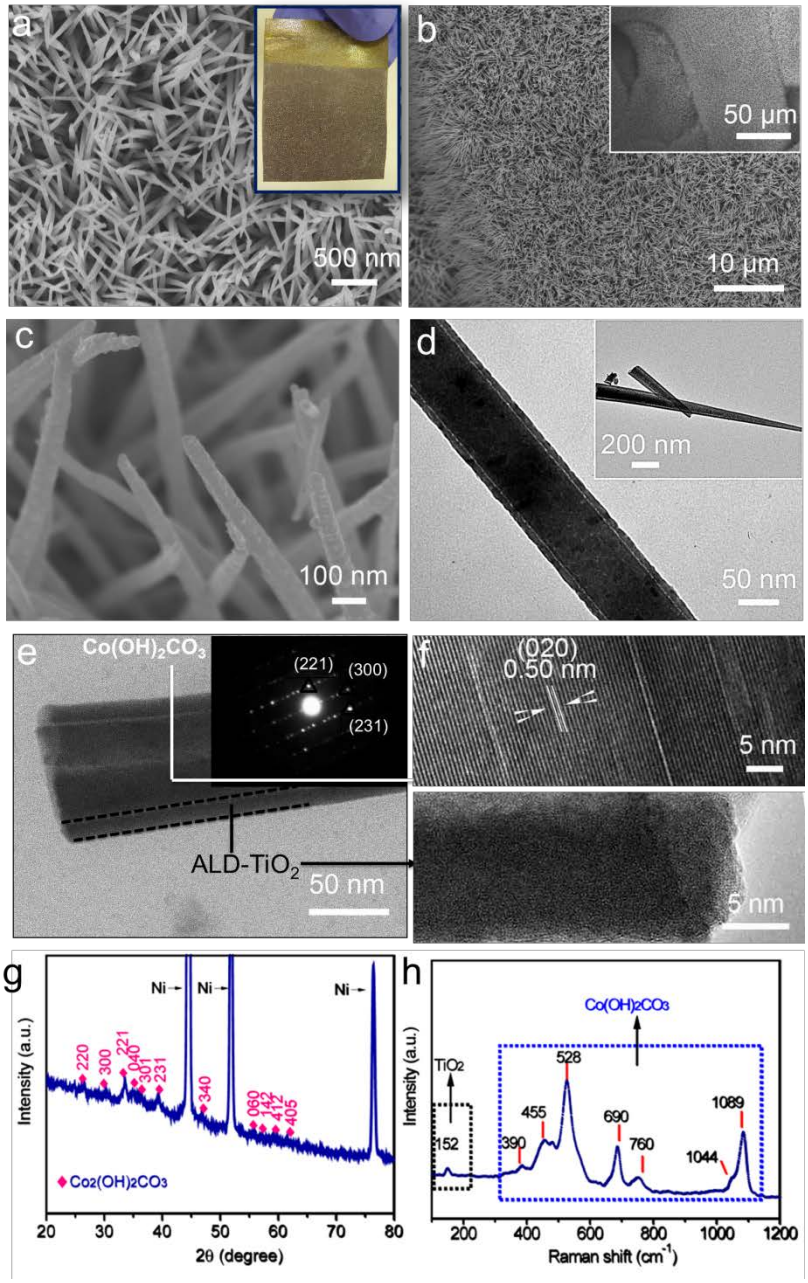

Figure S3. Morphology and microstructure characterizations of TiO_2@$Co(OH)_2CO_3$ core-shell arrays: (a-c) SEM images (photo of sample in inset); (d-f) TEM-HRTEM images (SAED pattern in inset); (g) XRD pattern; (h) Raman spectrum.

Only diffraction peaks of $Co(OH)_2CO_3$ (JCPDS 48-0083) are noticed and no peaks of TiO_2 are detected in the XRD pattern (**Figure S3**g), indicating the amorphous nature of ALD-TiO_2. Additionally, the co-existence of $Co(OH)_2CO_3$ and TiO_2 is verified in the Raman spectrum (**Figure S3**h). In addition to the Raman peaks of $Co_2(OH)_2CO_3$ (Figure S2h), a new characteristic peak of TiO_2 at 150 cm^{-1} is noted.

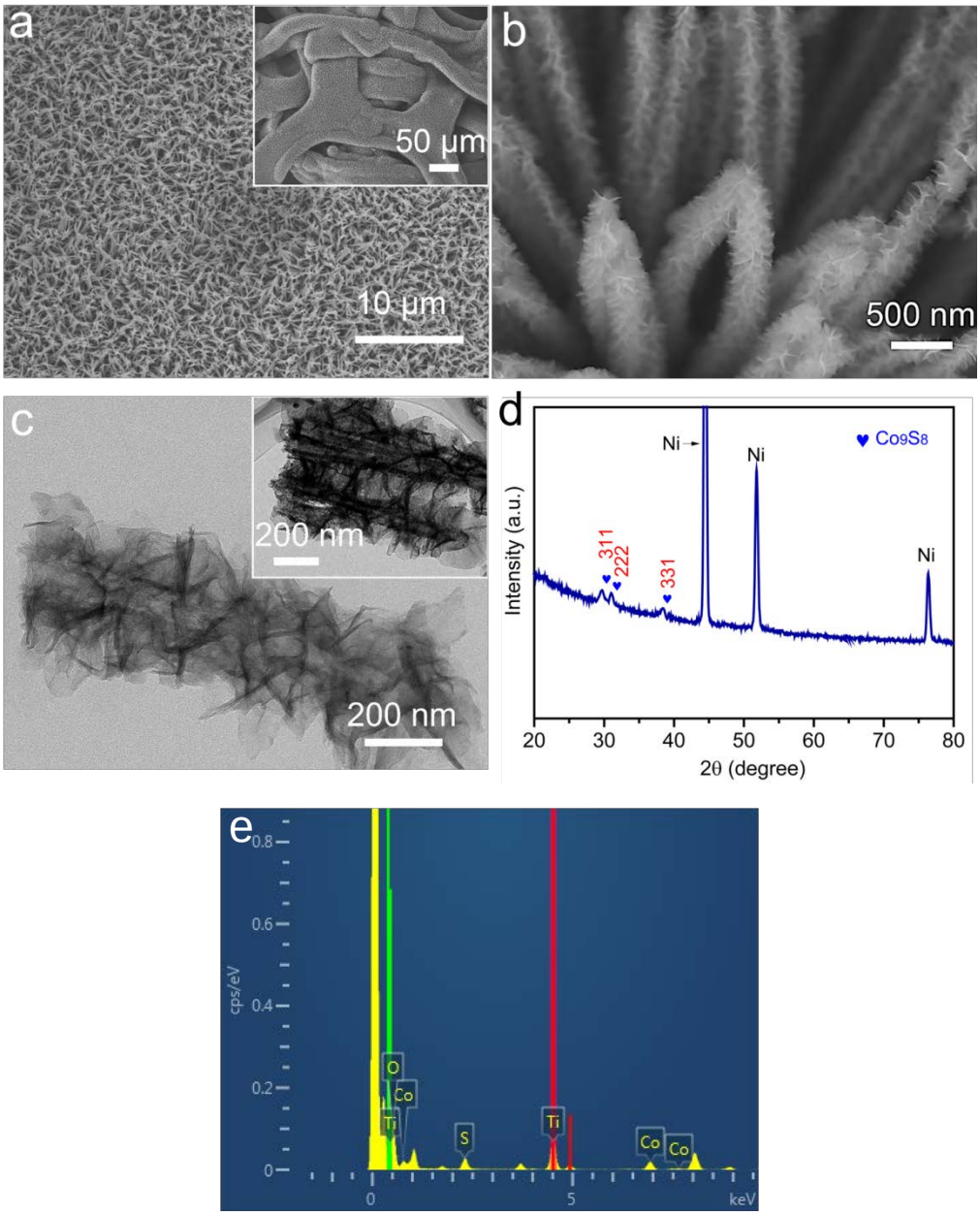

Figure S4. SEM-TEM images of TiO_2@Co_9S_8 hollow core-branch arrays on the nickel foam substrate: (a, b) SEM images; (c) TEM image (low-magnification TEM image in inset); and (d) XRD pattern; (e) EDS spectrum.

The diffraction peaks (311), (222), (331) and (531) in XRD pattern are indexed well with the crystal planes of Co_9S_8 phase (JCPDS 65-6801), indicating the successful synthesis of TiO_2@Co_9S_8 arrays on the nickel foam (**Figure S4**d). Also, the above results are supported by the EDS spectrum.

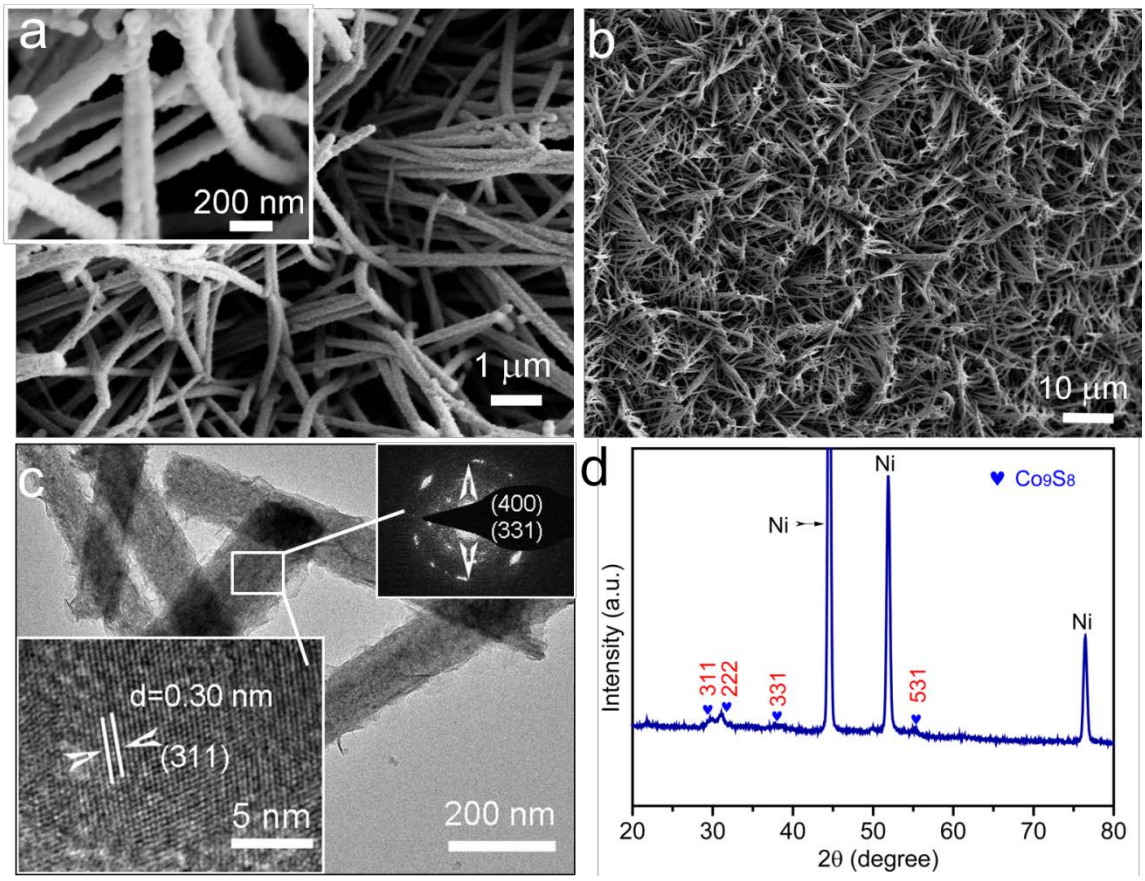

Figure S5. SEM-TEM images of Co_9S_8 nanowires arrays: (a-b) SEM images (inset: high-magnification SEM image); (c) TEM-HRTEM images (SAED pattern and HRTEM image in inset); (d) XRD pattern.

SEM images (**Figure S5**a-b) indicate the uniform distribution of Co_9S_8 nanowires on the nickel foam. TEM-HRTEM and SAED images (**Figure S5**c) reveal the formation of regular Co_9S_8 nanowires. The bright diffraction rings of (400) and (331) demonstrate the existence of high-crystalline Co_9S_8 phase (JCPDS 65-6801). And HRTEM image (inset in **Figure S5**c) exhibits the layer spacing of about 0.30 nm, which matches well with the (311) planes of Co_9S_8 phase, supported by the XRD pattern (JCPDS 65-6801).

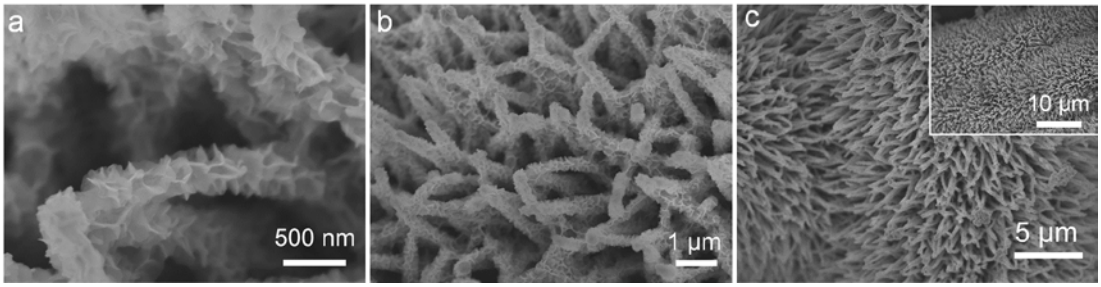

Figure S6. SEM images of TiO_2@Co_9S_8 hollow core-branch arrays grown on the carbon cloth substrate.

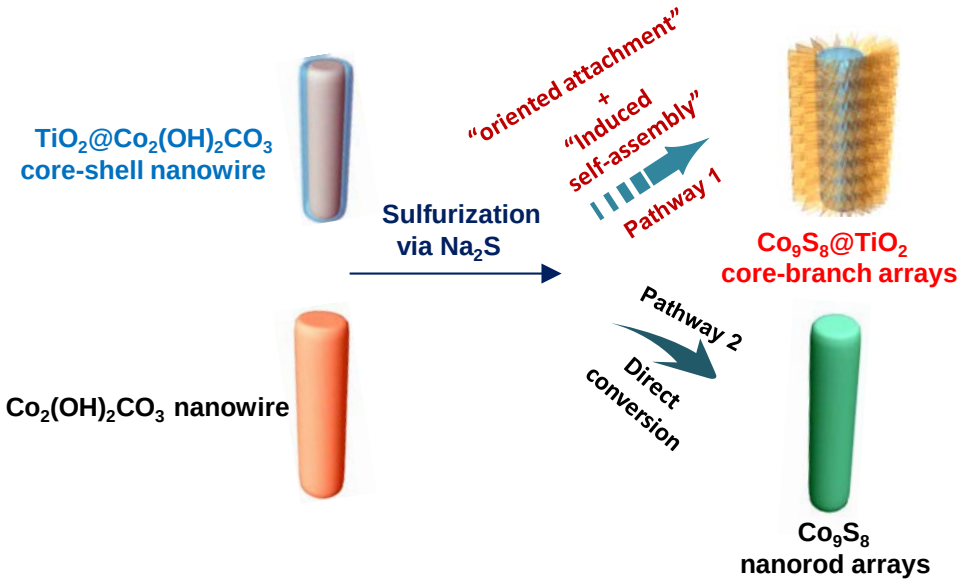

Figure S7. Schematic illustration of the synthesis of Co_9S_8@TiO_2 branch-core and Co9S8 nanowires arrays.

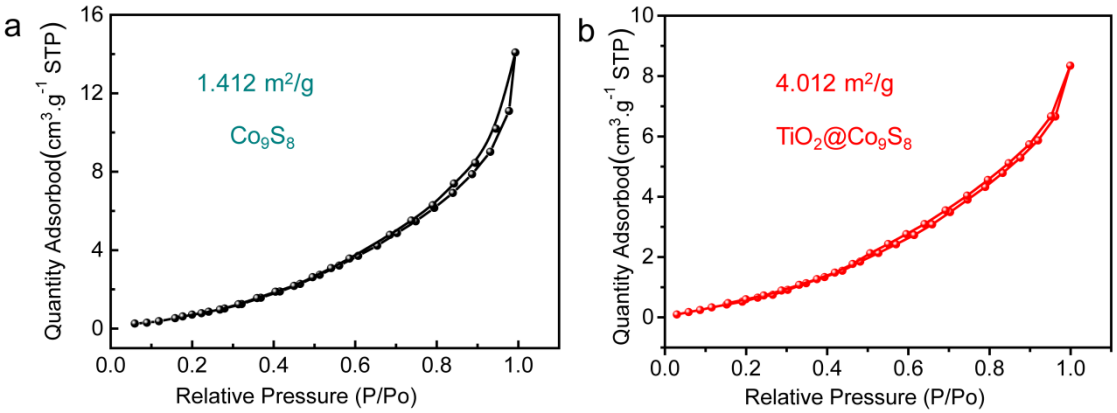

Figure S8. BET measurements: nitrogen adsorption-desorption isotherm curves: (a) Co_9S_8 nanowire arrays and (b) TiO_2@Co_9S_8 hollow core-branch arrays.

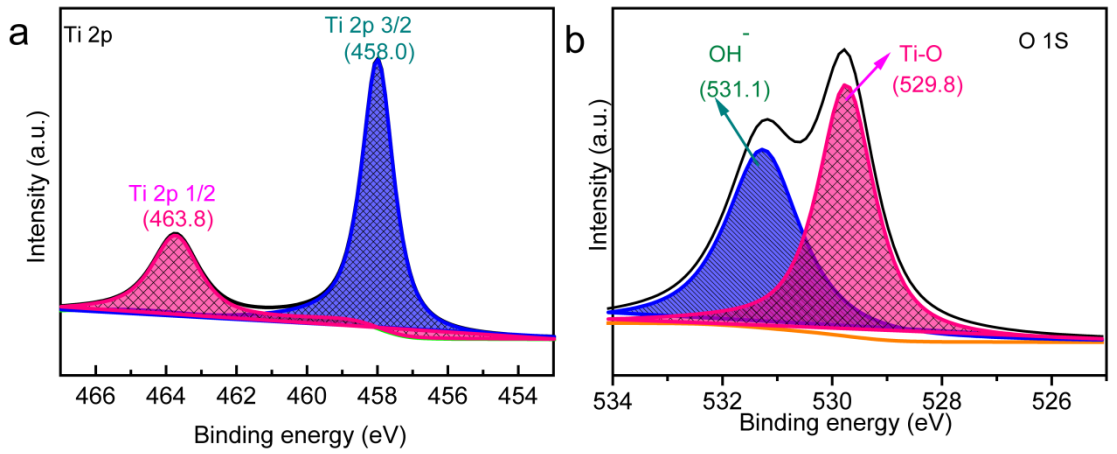

Figure S9. XPS spectra of O 1S and Ti 2p of TiO_2@Co_9S_8 arrays.

Two core levels Ti 2p1/2 (463.8 eV) and Ti 2p3/2 (458.0 eV) characteristic of TiO_2 are detected (**Figure S9**a).[1] Accordingly, Ti-O bond (529.8 eV) is noticed, while the peak at 531.1 eV belongs to OH^- (**Figure S9**b).[2]

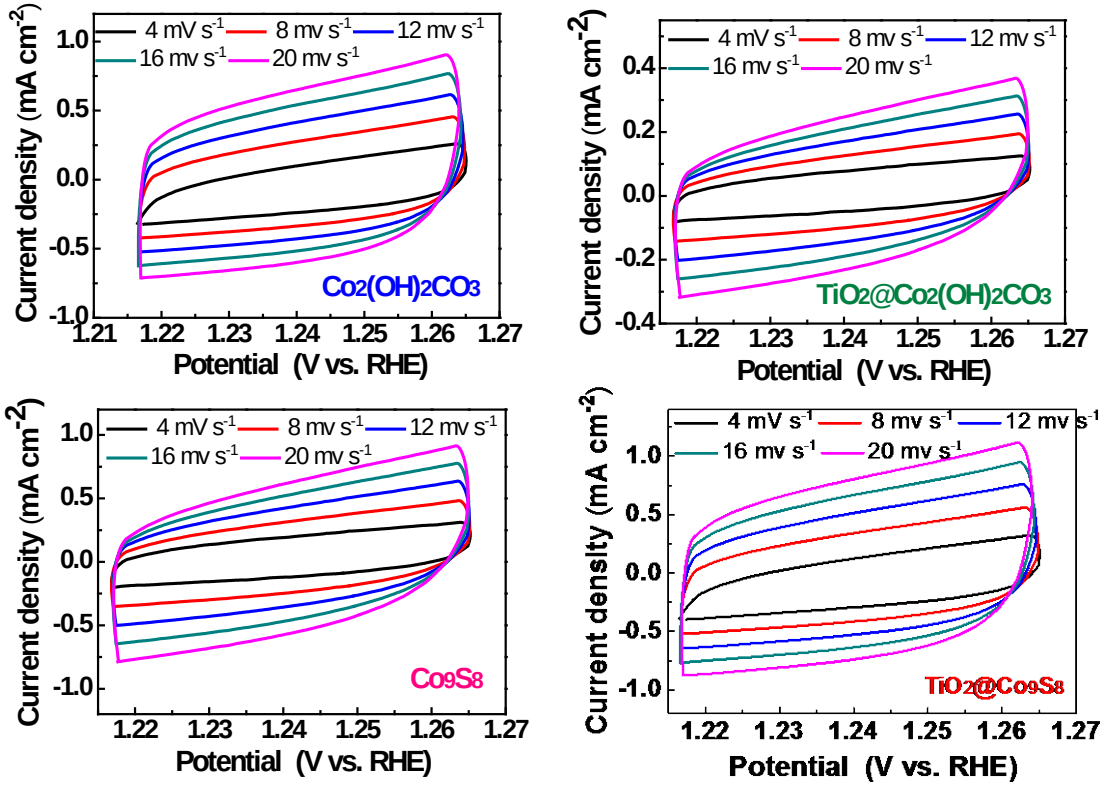

Figure S10. CV curves of different electrodes in double layer region at scan rates of 4, 8, 12, 16 and 20 mV s^{-1}, respectively.: (a) $Co_2(OH)_2CO_3$; (b) TiO_2@$Co(OH)_2CO_3$; (c)Co_9S_8; (d) TiO_2@Co_9S_8 electrodes.

Table S1 Electrocatalytic comparison for different catalysts

Catalyst	OER Overpotential (mV vs. RHE)	Tafel slope (mV Dec^{-1})	HER Overpotential (mV vs. RHE)	Tafel slope (mV Dec^{-1})	Ref.

$Co_2(OH)_2CO_3$	330	79	197	102	This work
$TiO_2@Co_2(OH)_2O_3$	350	89	226	126	This work
Co_9S_8	276	73	222	85	This work
$TiO_2@Co_9S_8$	240	55	139	65	This work
S-$CuCo_2O_4$	/	/	154	180	[3]
Co_9S_8@C	/	/	280	/	[4]
cobalt-sulfide	/	/	160	93	[5]
Co_2P nanorods	/	/	155	71	[6]
NiMo@N-C	/	/	130	84	[7]
NiFe@N-C	297	48	/	/	[7]
Co-P	345	42	94	47	[8]
Co_9S_8/graphene	409	82	/	/	[9]
Co_9S_8@N, S-C	310	68	/	/	[10]
Ni_3S_2 nanorods	157	159	/	/	[11]
NiS	290	89	140	83	[12]
NiFeS–Fe/NF	101	117	/	/	[13]
Ni_2P	290	/	/	/	[14]

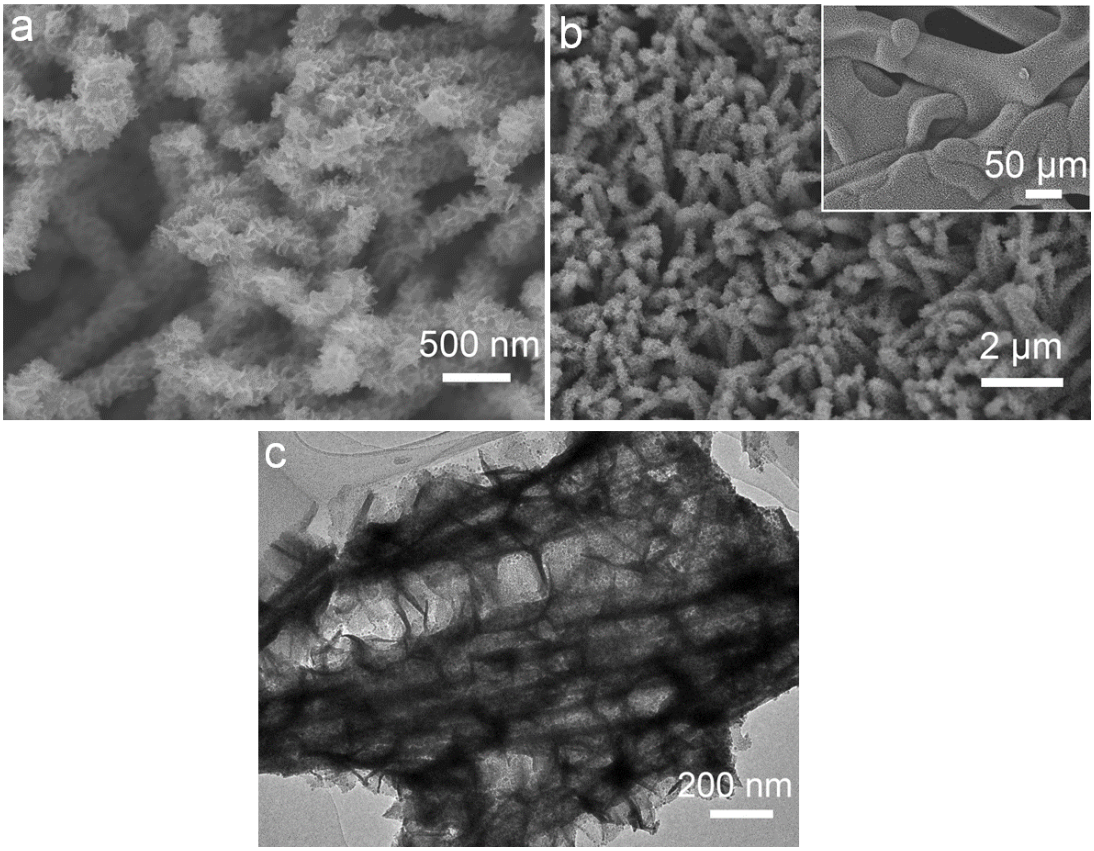

Figure S11. SEM images of $TiO_2@Co_9S_8$ electrode after 30 h test at 10 mA cm^{-2} during overall water splitting.

References

[1] X. Xia, Z. Zeng, X. Li, Y. Zhang, J. Tu, N. C. Fan, H. Zhang, H. J. Fan, *Nanoscale* **2013**, *5*, 6040.

[2] Y. Cong, J. Zhang, F. Chen, M. Anpo, *J. Phys. Chem. C* **2007**, *111*, 6976.

[3] Y. Gong, Y. Zhao, Y. Chen, Y. Wang, C. Sun, *RSC Adv.* **2016**, *6*, 43185.

[4] L.-L. Feng, G.-D. Li, Y. Liu, Y. Wu, H. Chen, Y. Wang, Y.-C. Zou, D. Wang, X. Zou, *ACS Appl. Mater. Interfaces* **2015**, *7*, 980.

[5] Y. Sun, C. Liu, D. C. Grauer, J. Yano, J. R. Long, P. Yang, C. J. Chang, *J. Am. Chem. Soc.* **2013**, *135*, 17699.

[6] Z. Huang, Z. Chen, Z. Chen, C. Lv, M. G. Humphrey, C. Zhang, *Nano Energy* **2014**, *9*, 373.

[7] Y. Zhang, X. Xia, X. Cao, B. Zhang, N. H. Tiep, H. He, S. Chen, Y. Huang, H. J. Fan, *Adv. Energy Mater.* **2017**.

[8] N. Jiang, B. You, M. Sheng, Y. Sun, *Angewandte Chemie* **2015**, *127*, 6349.

[9] S. Dou, L. Tao, J. Huo, S. Wang, L. Dai, *Energy Environ. Sci.* **2016**, *9*, 1320.

[10] H.-x. Zhong, K. Li, Q. Zhang, J. Wang, F.-l. Meng, Z.-j. Wu, J.-m. Yan, X.-b. Zhang, *NPG Asia Mater.* **2016**, *8*, e308.

[11] W. Zhou, X.-J. Wu, X. Cao, X. Huang, C. Tan, J. Tian, H. Liu, J. Wang, H. Zhang, *Energy Environ. Sci.* **2013**, *6*, 2921.

[12] W. Zhu, X. Yue, W. Zhang, S. Yu, Y. Zhang, J. Wang, J. Wang, *Chem. Commun.* **2016**, *52*, 1486.

[13] B. Dong, X. Zhao, G.-Q. Han, X. Li, X. Shang, Y.-R. Liu, W.-H. Hu, Y.-M. Chai, H. Zhao, C.-G. Liu, *J. Mater. Chem. A* **2016**, *4*, 13499.

[14] L.-A. Stern, L. Feng, F. Song, X. Hu, *Energy Environ. Sci.* **2015**, *8*, 2347.